Nanoscale

PAPER

View Article Online
View Journal | View Issue

Cite this: *Nanoscale*, 2023, **15**, 5001

Combining negative photoconductivity and resistive switching towards in-memory logic operations†

Subham Paramanik[a] and Amlan J. Pal *[a,b]

A family of rudorffites based on silver-bismuth-iodide shows a transition from a conventional positive photoconductivity (PPC) to an unusual negative photoconductivity (NPC) upon variation in the precursor stoichiometry while forming the rudorffites. The NPC has arisen in silver-rich rudorffites due to the generation of illumination-induced trap-states which prompted the recombination of charge carriers and thereby a decrease in the conductivity of the compounds. In addition to photoconductivity, sandwiched devices based on all the rudorffites exhibited resistive switching between a pristine high resistive state (HRS) and a low resistive state (LRS) under a suitable voltage pulse; the switching process, which is reversible, is associated with a memory phenomenon. The devices based on NPC-exhibiting rudorffites switched to the HRS under illumination as well. That is, the resistive state of the devices could be controlled through both electrical and optical inputs. We employed such interesting optoelectronic properties of NPC-exhibiting rudorffites to exhibit OR logic gate operation. Because the devices could function as a logic gate and store the resistive state as well, we concluded that the materials could be an ideal candidate for in-memory logic operations.

Received 18th January 2023,
Accepted 24th January 2023

DOI: 10.1039/d3nr00278k

rsc.li/nanoscale

1. Introduction

In optoelectronics, the light-induced charge carrier generation, that is, enhancement of electrical conductivity under illumination is quite common in most semiconductors and is referred to as positive photoconductivity (PPC). In contrast, this rule is not followed in a few semiconductors, where illumination results in a decrease in the conductivity below the dark level, leading to a negative photoconductivity (NPC) behavior.[1–3] This anomalous photoconductivity was initially observed in some well-studied materials in their low-dimensional forms, such as silver and silicon nanowires,[4,5] indium nitride (InN) thin films,[6] indium arsenide (InAs) nanowires,[7] single-layered molybdenum disulfide (MoS_2),[1,8,9] and other few-layered 2D materials, such as graphene, platinum diselenides, and rhenium diselenides.[10–13] However, there has been no consensus regarding the mechanism of NPC in the materials. It is believed that enhanced recombination of majority carriers and/or scattering of charge carriers during the transport may be the rationale for yielding the NPC.[3] Despite the importance and interest toward the NPC phenomenon, the complex characterization conditions in the form of measurements at low temperatures and/or under an ultrahigh vacuum condition limited their development and prompted researchers to look for newer compounds to achieve an NPC under ambient conditions.[1,12] In this direction, a few halide perovskites have recently exhibited NPCs at room temperature. For example, as the first report on halide perovskites, Hague *et al.* reported that the photoconductivity of methylammonium lead bromide upon bismuth doping changed from a PPC to an NPC due to the formation of photo-generated DX-like defect centers (D: donor atom; X: unspecified lattice defect) acting as recombination sites for the carrier conduction process.[14] Soon, other halide perovskites in the form of $CsPbBr_3$/graphene heterojunctions,[15] $CsPbX_3$-ITO nano-heterojunctions (NHJs),[16] and lead-free perovskites such as $Cs_3Bi_2Br_9$ films and $Cs_3Bi_2Cl_9$ single crystals[17,18] were reported to exhibit NPCs. Despite the easy processability of some of the halide perovskites, several materials necessitated complex device architectures to yield an NPC behavior.[16,19] Introducing defect states through doping while yielding a transition from a positive to a negative photoconductivity also altered the optical bandgap of perovskites;[14] a change in the bandgap upon doping would hence have led to a disparity in the photoresponse and unequal photo-activity in different wavelength limits.

[a]*School of Physical Sciences, Indian Association for the Cultivation of Science, Jadavpur, Kolkata 700032, India. E-mail: sspajp@iacs.res.in*
[b]*UGC-DAE Consortium for Scientific Research, University Campus, Khandwa Road, Indore 452001, India*

† Electronic supplementary information (ESI) available. See DOI: https://doi.org/10.1039/d3nr00278k

In the context of resistive switching and its associated memory phenomenon, a range of halide perovskites exhibit such properties.[20–22] Of late, they are also being considered for synaptic functions.[23–25] The underlying mechanism can be described as either filamentary (formation of metal or metal-like conducting bridges) or interfacial type (modulation of the Schottky barrier and trapping-detrapping of the charge carriers).[20,26] In this respect, the use of NPC-exhibiting materials in resistive switching devices may add an extra dimension to the memory devices. In other words, a combination of electrical and optical stimuli as independent inputs can then be considered for memristive devices in controlling their resistive states. In this work, we envisaged such a combination as a step forward toward the realization of in-memory logic operations. It may be recalled that in-memory computing requires memory elements in the processor to carry out the logic operations as well. Such an approach puts aside the two-way data transfers, namely, retrieving data from the memory to the processor for processing and then transferring it back to the memory upon computation. Conventional memory elements are separated from the processor leading to the von Neumann bottleneck, which refers to the slowness of data transfers between the memory elements and the processor.[27–30] The bottleneck has necessitated the formation of elements as in-memory logic gates where the memory elements will carry out the logic operations as well. That is, in-memory logic computing has turned out to be necessary to overcome the von Neumann bottleneck.

In the present work, we have considered rudorffites from the silver-bismuth-iodide family ($Ag_mBi_nI_{m+3n}$ with m and n being integers).[31,32] While such compounds exhibit resistive switching through an electrical stimulus and an associated memory phenomenon, we show that upon a change in the composition, the material exhibits a transition in the photoconductivity between a PPC and an NPC without a change in the optical bandgap. The NPC-exhibiting devices could hence be switched to a high-resistive state (reverse switching) through the application of optical illumination as well. The introduction of this optically erasable character in memory devices has brought an additional parameter in the process of resistive-switching and memristive functionalities. Such functionalities of the materials/devices have therefore enabled us to consider a combination of electrical and optical stimuli as independent inputs for controlling the output, that is, the resistive state of optoelectronic memristive devices. We could finally establish that the NPC-exhibiting-rudorffite may be an ideal candidate for evidencing in-memory logic operation; the nonvolatile memory element has functioned for OR gate logic operation and stored the resistive state as well.

2. Results and discussion

2.1. Negative photoconductivity

We earlier reported the optical and structural characteristics of the rudorffite compounds in the $A_mB_nX_{m+3n}$ series formed through control over the precursor stoichiometry. By combining Kelvin probe force microscopy (KPFM) and scanning tunneling spectroscopy (STS) studies in Ag_3BiI_6, Ag_2BiI_5, $AgBiI_4$, $AgBi_2I_7$, and $AgBi_3I_{10}$, a gradual change in the electronic conductivity from a p-type to an n-type was observed; in addition, a shift in the conduction band (CB) and the valence band (VB) edges with respect to the Fermi level (E_F) was also witnessed across the series of the compounds, although the transport gap remained unaltered.[33] The variations in the type of electronic conductivity and the shift in the band-edges have arisen due to the presence of different types of charged point defects created under different film-forming conditions. It is now envisaged that different types of defects along with the variation in the E_F and band-energies may have an impact on the (type of) photoconductivity of the materials.

We thereby proceeded to characterize the devices under dark and 1 sun illumination conditions. The structural and optical characteristics of the materials and their thin films have been presented in the ESI and also in Fig. S1–S3.† The optical band gap of these compounds, as derived from the Tauc plots (Fig. S1b†), was around 1.8 eV and remained invariant for all the compounds. A schematic diagram of the sandwiched structure and photographs of the devices have been presented in Fig. 1a and b, respectively. In Fig. 1c, we have presented current–voltage (I–V) characteristics of different ITO/$Ag_mBi_nI_{m+3n}$/PMMA/Al devices under the two conditions. The I–Vs recorded under both conditions were nonlinear in nature implying metal–semiconductor Schottky contacts in the devices. When we compare the I–Vs recorded in repetition under a dark (or illumination) condition, no sign of device degradation was observed. The device-to-device variation in current under dark and illumination conditions was low (Fig. S4†). When the I–Vs under the illumination condition are compared with the dark characteristics, a positive photoconductivity (PPC) is evidenced in devices based on $AgBiI_4$ and $AgBi_2I_7$. The current at a particular voltage shows a large increase as compared to that under a dark condition. This behavior is quite conventional in devices based on halide perovskites and can be attributed to be due to photoinduced carrier generations under illumination. The devices based on a silver-rich rudorffite (Ag_2BiI_5), on the other hand, exhibited a negative photoconductivity (NPC). Such behavior is quite uncommon and is observed only in a handful of materials where the conduction process involves photoinduced defect-states which can take part in the trapping and recombination processes of photogenerated carriers.[3,14] Some 2D-material-based systems have also exhibited a similar NPC behavior due to the photogating effect or adsorption/desorption of oxygen and water molecules at the interface under illumination.[34]

To further shed light on the emergence of an NPC, transient photocurrent measurements were carried out. To do so, the device current was measured at 0.7 V and the illumination was sequenced between an off- and an on-state in repetition with the help of a mechanical shutter. In Fig. 1d, we present the transient current output from devices based on the rudorffites. The compounds responded differently in the tran-

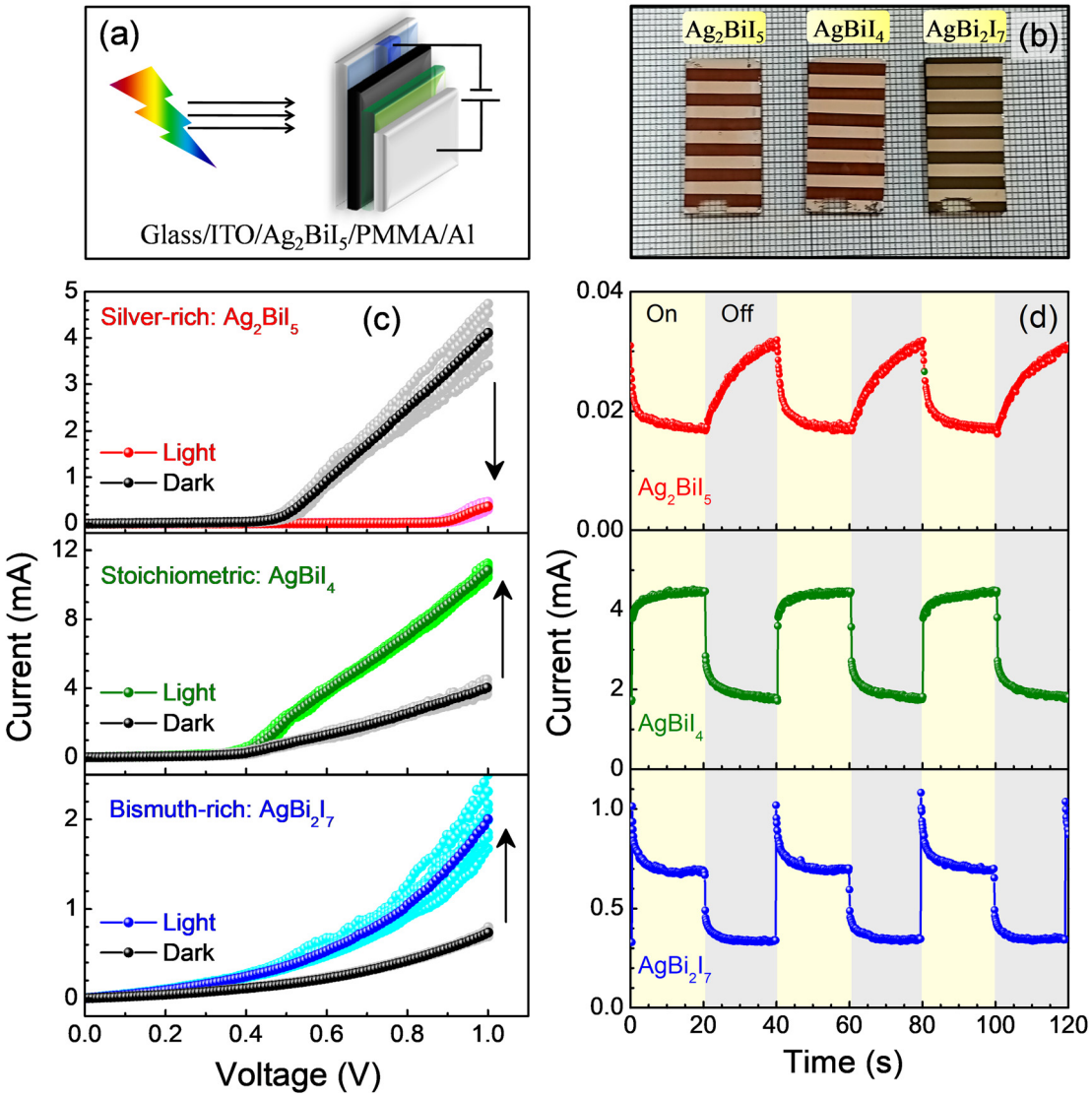

Fig. 1 (a) A schematic diagram of a sandwiched structure and (b) photographs of the devices. (c) Current *versus* voltage characteristics of sandwiched devices based on the rudorffites (as mentioned in the legend) under a dark and an illuminated condition; while the *I*–*V*s recorded in repetition are presented, the average *I*–*V* characteristics are presented through dark symbols. (d) Transient photoconductivity measurements of the devices; the current was recorded at 0.7 V by turning-on the illumination for 20 s with a 50% duty cycle in a repeated sequence.

sient photoconductivity measurements. In the $AgBiI_4$ compound formed through the use of stoichiometric precursors, the rise of the photocurrent under illumination was conventional; the photocurrent exhibited a sharp increase followed by an upward saturating behavior. Upon removal of the illumination, the device current decayed back to the dark current level (Fig. 1d: middle panel). Such behavior is typical in PPC-exhibiting materials. On moving to both silver-rich and bismuth-rich rudorffites, the nature of transient photoconductivity changed drastically. For the bismuth-rich compound ($AgBi_2I_7$), which exhibited a PPC although, the photocurrent showed a sharp increase at the turn-on point of the illumination followed by a slow decay to a stable value, which was much higher than the dark current. The behavior in the transient photocurrent implies the presence and involvement of a large number of intrinsic defect states in the rudorffite layer that is capable of trapping the photogenerated carriers. Here, quick generation of charge carriers upon illumination increases the current sharply followed by partial trapping of photogenerated carriers due to a large number of intrinsic charged point defects, resulting in slow decay of the photocurrent to a steady value representative of a PPC. On removing the illumination, the photocurrent traced back to the level of the dark current (Fig. 1d: lower panel). In both the rudorffites, the transient photocurrent behavior was repeatable over illumination cycles.

The negative photocurrent observed in devices based on the silver-rich rudorffite, Ag_2BiI_5, was also manifested in transient photoconductivity measurements (Fig. 1d, upper panel). Under the illumination, the photocurrent decayed far below the dark current level and, on the removal of illumination, the

current recovered (increased) to the level observed under the dark condition, albeit at a slower pace. The longer recovery time suggests the metastable nature of the trap states. In general, the defect states in halide perovskites are shallow and are feebly capable of trapping the charge carriers. In this situation, we hypothesize a similar mechanism to that described in hybrid halide perovskites;[14,35] the optical illumination activates the metastable states to become energetically stable. Upon turning the illumination off, these defect states become unstable again and the majority of the metastable states that were accumulated under exposure dissipate away through a self-healing process. This hypothesis is also supported by the enhanced Urbach tailing in the materials upon prolonged exposure. A significant increase in the Urbach energy upon illumination and subsequent slow self-healing in the dark have been observed (Fig. S5†). Such a slow recovery process in materials exhibiting an NPC is also in agreement with earlier reports.[14,17,36]

When the photoconductivity yield (Y_{PC}) of a device was calculated through a conventional relationship:

$$Y_{PC} = (I - I_{dark})/I_{dark} \quad (1)$$

the yield could be found to be around +200% for devices exhibiting a PPC. The increase in the current upon illumination remained expectedly linear with the intensity of light. The Y_{PC} was −100% in the device based on the material possessing an NPC and was found to be independent of the light intensity in the range of 0.1 to 1 sun. While a higher yield than the present report has been obtained in other PPC-exhibiting materials, it is noteworthy to state that the negative Y_{PC} achieved in devices based on Ag_2BiI_5 is one of the highest reported so far.[14]

When the results on the series of rudorffites are compared, the different natures of photoconductivity could be analyzed in terms of the antagonism between the type of defect states and the density of photogenerated charge carriers. For the bismuth-rich rudorffite ($AgBi_2I_7$) and the one formed with stoichiometric precursors ($AgBiI_4$), the iodine vacancies (V_I) have the lowest formation energy and result in n-type electronic conductivity in the compounds.[33,37] Upon illumination and thereby photogeneration of carriers, the easily accessible vacancies are passivated leading to an increased density of uncompensated photogenerated charge carriers and resulting in PPC in the rudorffites.

In the case of the silver-rich rudorffite (Ag_2BiI_5), silver vacancies (V_{Ag}), due to their lower formation energy, dominate in the compounds over the other possible defects and result in a p-type electronic conductivity. The nature of conductivity was obtained from the absolute energy landscape of the compounds as derived from STS and KPFM measurements;[32] from the proximity of VB-edge with respect to the Fermi energy as compared to the CB-edge, we inferred the p-type nature in the silver-rich perovskites. These vacancies are shielded by iodides in the [AgI_6] octahedra and their facile passivation may not occur upon photogeneration. Such an inference is also supported by the higher activation energy of silver vacancies as compared to the iodine vacancies.[37] The density of uncompensated photogenerated charge carriers hence does not increase. On the other hand, the trap-states generated under illumination start to dominate the conduction process, prompt recombination of charge carriers, decrease the conductivity thereby, and hence yield an NPC behavior in the compound.

Such a mechanism of NPC should lead to a decay of photocurrent in a biexponential manner involving (1) the formation of charged defect-states and (2) the trapping and recombination processes of photogenerated carriers.[14] The decay characteristics of photocurrent at a time t under illumination could thereby be fitted to:

$$I(t) = I_0 + A_1 e^{\frac{-t}{t_1}} + A_2 e^{\frac{-t}{t_2}} \quad (2)$$

where I_0 represents the device current prior to the illumination, t_1 and t_2 represent the two time constants involving the two processes, and A_1 and A_2 are constants. The experimental results have yielded 1.2 s and ~15 s as the two time constants (Fig. 2a). This clearly signifies that two mutually independent phenomena are contributing to the overall decrease in current under illumination. It can be presumed that the smaller time constant (t_1) is associated with a quick generation of trap states followed by a delayed trapping process with a larger time constant (t_2).[38] In contrast, the device based on the bismuth-rich rudorffite exhibited a single exponential decay while reaching the steady state of the photocurrent (Fig. S6†) representing the involvement of intrinsic trap states in the material towards the recombination process.

The aforesaid mechanism for an NPC in Ag_2BiI_5 can further be supported by studying the conduction mechanism under dark and illumination conditions. To infer the mechanism, we have presented the *I–V*s in a double-logarithmic scale (Fig. 2b). While the slope of the plots was linear in the small field region implying domination of the Ohmic conduction process, the slope rose to a much higher value (>3) in the high-field regime (trap-filled limited conduction, TFL). Beyond a threshold voltage (V_{TFL}), where all the trap states are filled by charge carriers, the current increases with such a high slope, and the device is said to be operating in the TFL conduction region. The trap density (N_{trap}) in the device could thereby be calculated from a measure of V_{TFL} using the relationship:

$$N_{trap} = \frac{2V_{TFL}\varepsilon\varepsilon_0}{eL^2} \quad (3)$$

where ε is the relative dielectric constant of the material, ε_0 is the vacuum permittivity, e is the electronic charge, and L is the thickness of the active material.[39,40] Fig. 2b shows that the V_{TFL} of the device moves to the higher voltage under illumination suggesting a significant increase in the active trap densities in the material. On the other hand, no such change in the V_{TFL} was observed in devices based on PPC-exhibiting materials, $AgBiI_4$ and $AgBi_2I_7$ (Fig. S7†). The results hence support the active role of the photogenerated trap states in attaining the NPC in Ag_2BiI_5.

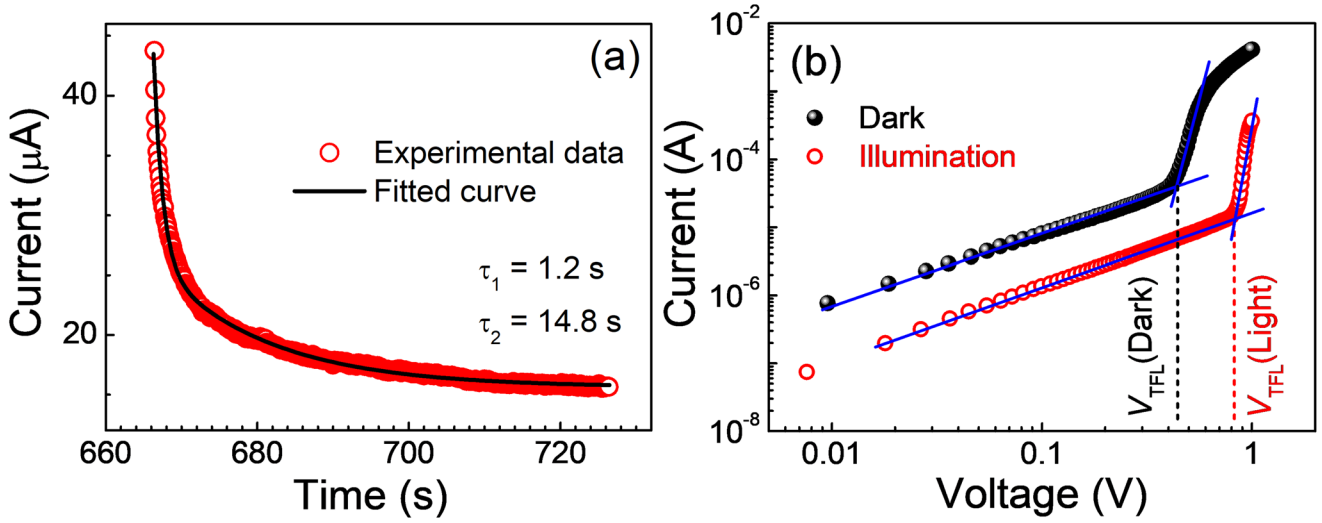

Fig. 2 (a) Decay characteristics of the photocurrent of a device based on Ag_2BiI_5 and (b) current–voltage characteristics of the device under dark and illumination conditions in a double-logarithmic scale.

It can be intriguing to introduce NPC-exhibiting materials in memristive devices so that their resistive states can also be modulated with another input, that is, optical illumination. In conventional memristive devices, both write and erase operations are accomplished by electrical pulses. With the introduction of an optical stimulus as an input, a combination of electrical and optical inputs can be considered in memristive devices for controlling their resistive states toward in-memory logic operations.

2.2. Memristive behavior

We then proceeded to characterize the devices based on Ag_2BiI_5 for their memristive properties. To study the conventional memristive behavior, we have considered the same device configuration, that is, ITO/Ag_2BiI_5/PMMA/Al (Fig. 1a). The ultrathin-film of PMMA below the aluminum electrode acted as a protective layer to forbid aluminum ion migration upon application of a bias and thereby the formation of metal filaments, which often give rise to resistive switching due to the make-and-break of filaments. The devices were first characterized under a dark condition. Fig. 3a shows the *I*–*V* characteristics of a device based on Ag_2BiI_5, which exhibited an NPC, under the application of a voltage in multiple bipolar sweeps between −2.0 and +2.0 V in loops. In the positive voltage, the device exhibited two distinct resistive states. The device, which was in a pristine or a high resistive state (HRS), switched to a low resistive state (LRS) beyond a positive voltage. The retention of the LRS was nonvolatile in nature as manifested by the *I*–*V*s in the +2.0 to 0 V sweep; the LRS could be seen to be retained during the trace. To reset the LRS to an HRS, a negative voltage was required; the reset voltage was as low as −0.2 V. The two states can be achieved reversibly during the multiple sweeps of the *I*–*V* characteristics (Fig. 3a). The resistive switching process in Ag_2BiI_5 can be explained through a well-established mechanism of trapping and detrapping of charge carriers in the interfacial defect states (Fig. S8 and the discussion thereof†); such a mechanism has been considered to explain the resistive switching in devices based on a range of oxide and perovskite materials.[26,41]

To test the retention of the two resistive states, the device was subjected to a pulse programming method (inset of Fig. 3b) with a write pulse (V_{Write} = 2.0 V, 100 ms) or an erase pulse (V_{Erase} = −1.0 V, 100 ms) followed by data readout under a train of small read voltage pulse (V_{Read} = 0.2 V, 100 ms, duty cycle = 9%). The current at the read voltage depended on the preceding write or erase voltage and was different and clearly separable. That is, the state of the device could be probed by measuring the current under the read voltage; the device could be found to retain its resistive state for more than 90 min exhibiting decent data retention without any significant deterioration of either of the states (Fig. 3b).

The two resistive states of the device could also be flipped as well. The sequence of voltage pulse for such measurements has been (i) a write pulse, (ii) data readout, (iii) a reset pulse, and (iv) data readout, in sequence (inset of Fig. 3c). The magnitude and the width of the pulses that were used for data retention characteristics were alike. The current under the data readout for more than 1500 repeating sequences was clearly dependent on the preceding voltage pulse (Fig. 3c). The results hence infer that the device could also be switched between an LRS and an HRS reproducibly, and the state can be read over a large number of switching cycles. The energy consumption of the devices was around 0.5 μJ as calculated through $E = IVt_d$, where *I*, *V*, and t_d are the device current, applied voltage, and the width of the switching pulse, respectively; the set and the reset voltages of the devices were low as compared to the reported results (Table S1†).

The devices based on $AgBiI_4$, which exhibited a PPC, manifested a mostly identical memristive character. The *I*–*V* plots under a voltage sweep applied in multiple loops, the data

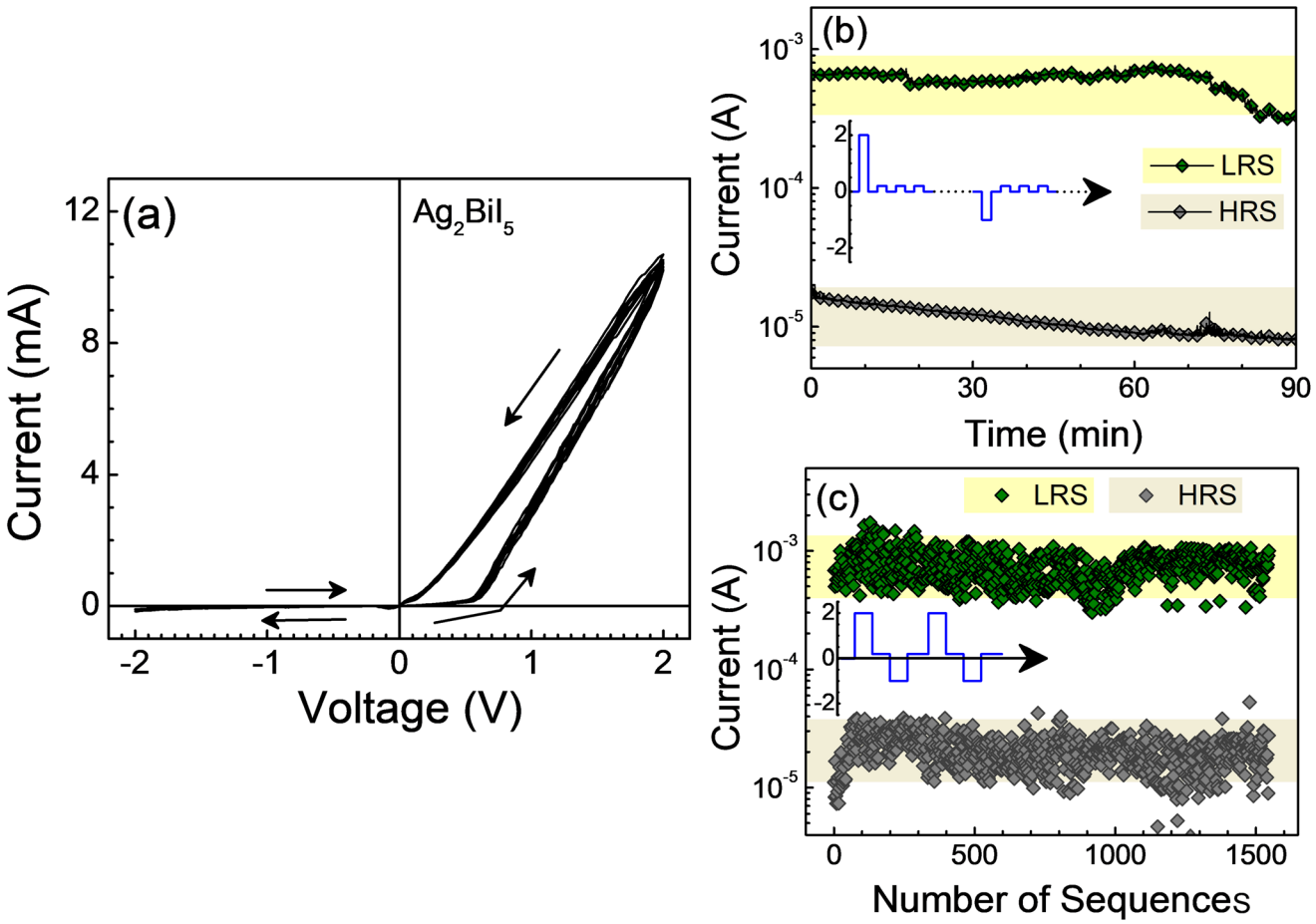

Fig. 3 (a) Current–voltage characteristics of the device based on Ag_2BiI_5 under the application of a voltage in multiple loops under dark conditions. (b) and (c) represents the current output of the LRS and HRS under a train of 0.2 V voltage pulse to study the data retention and cyclic endurance of the devices, respectively. The LRS and HRS were induced by applying +2.0 and −1.0 V, respectively; the scheme of voltage pulse used in the measurements is shown in the inset of the respective figures.

retention and cyclic endurance characteristics of the device are shown in Fig. S9.†

2.3. Combining NPC and memristor: in-memory logic gates

We then characterized the devices under an illumination condition for memristive applications. Due to the photoinduced generation of trap-states and hence the NPC character of the material, the resistance of a device based on Ag_2BiI_5 in its LRS could now be reset to the pristine HRS without the need for a reverse voltage; that is, the illumination can also be considered as a parameter to induce the HRS. Such a property has been shown in Fig. 4 when the devices were put to an LRS with a voltage pulse and then to an HRS with an optical illumination. The two states could separately be probed under the usual train of +0.2 V read voltage as a function of time (Fig. 4a). The current under the read voltage was distinctly different representing the LRS and the HRS induced by a +2.0 V and an illumination, respectively. An optically switched HRS could also be flipped to an LRS through an electrical pulse; the bias required for such a process (~0.9 V) is however higher than the initial switching voltage under the dark conditions (~0.5 V). The trap-states generated under illumination demanded a higher injected carrier density and thereby a higher voltage to compensate for the photogenerated trap-states in switching the device to an LRS.

The states could also be flipped in cycles over a large number of switching cycles (Fig. 4b), where a +2.0 V pulse and an illumination were imposed on the device in sequence and each was followed by a read-voltage (+0.2 V) to probe the imposed state. Such a phenomenon can thereby be referred to as an optical reset character. This property has earlier been observed in $Cs_3Bi_2Cl_9$.[42] With this particular characteristic, the illumination can be considered to act as an independent input for resistive switching to an HRS, while the voltage remained the input to switch the device to an LRS under +2.0 V and to an HRS (under −1.0 V). We may hence summarize that the resistive switching devices based on a material possessing an NPC property can be switched to an LRS through the application of a suitable voltage pulse; they can be reset or switched back to the HRS through the application of either a reverse

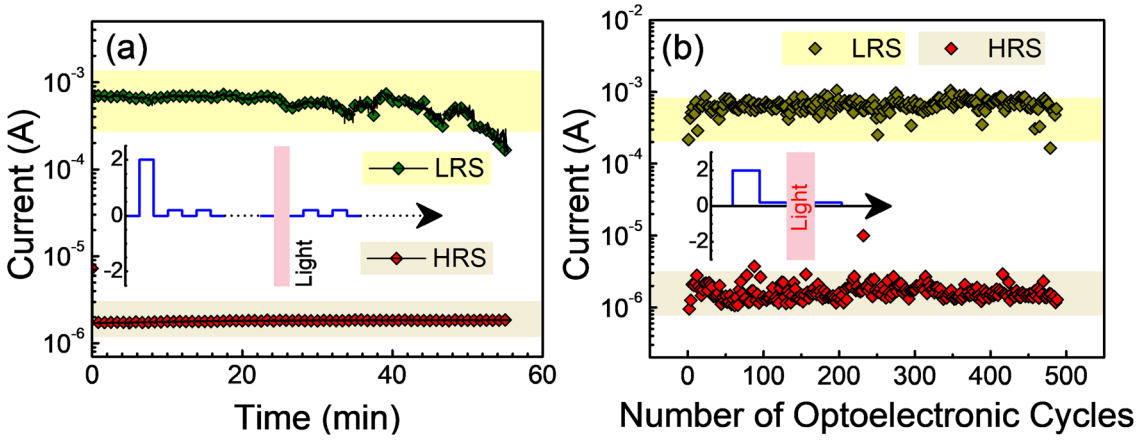

Fig. 4 The current output of a device based on Ag_2BiI_5 under a +0.2 V voltage pulse (a) after an LRS or an HRS was induced by a +2.0 V pulse and an illumination, respectively and (b) when the two states were imposed by a combination of +2.0 V pulse and illumination and then flipped in sequence to study the cyclic reproducibility; the states were probed with a read voltage of +0.2 V after each input. The sequence of the write voltage pulse, the illumination, and the read voltage are shown in the respective insets. While the 1 sun illumination was shined for 1 s, the width of the write and read voltage pulses was 100 ms.

voltage pulse or illumination. It can however be stated that the conventional voltage-controlled multilevel memory devices are associated with a complex geometry and compliance circuitries, whereas the optical coupling in the present devices is completely free from such complexities. Moreover, the optically erasable character results in less fluctuation in probing the resistive states (Fig. 4b) as compared to the electrical one (Fig. 3c). The optical stimulus does not produce high current and Joule heating in the devices during the erase process and hence can be considered to be energy-efficient compared to conventional voltage-controlled memory devices.

The combination of electrical and optical stimuli to a memristive device has arisen interesting optoelectronic properties. They in fact exhibit an in-memory OR logic gate operation! In this optoelectronic logic gate, the applied voltage and the illumination are considered two independent inputs. As the first input, a voltage pulse of +2.0 V (100 ms) and −1.0 V (100 ms) are treated as "0" and "1", respectively. We can naturally term the dark and the illumination conditions as "0" and "1", respectively, as the second input. The inputs have been represented in a tabular form in Fig. 5a. When we consider the resistive state of the device as the output of the logic gate, we find that the device is in the LRS if a +2.0 V (100 ms) is applied and the device is probed under a dark condition (input: 00). If a −1.0 V (100 ms) voltage is applied in dark (input: 10), or only illumination is shined (input: 01), or both are imposed (input: 11), the output would represent an HRS (Fig. 5b). In this figure, we have presented the device current at +0.2 V under the different combinations of the two inputs in sequence. The current could be found to be high under the (00) input condition implying an LRS; the current has been low, that is, the device is in an HRS, under the other three input conditions, namely (10), (01), and (11). In Fig. 5c, we have presented the average resistance (low or high) over many measurements and the corresponding resistive state under the four conditions of the two inputs in the form of a truth table. The combination of two inputs and the output represented an OR logic gate. The output, which represented the "state" of the device, has been nonvolatile in nature. The box-chart plot showing the distribution of the device resistance under the application of the two inputs in different combinations is presented in Fig. 5d. The output resistance of the "0" and "1" states representing an LRS and an HRS, respectively, differed by more than 2 orders of magnitude (Fig. 5d). That is, a nonvolatile OR logic gate could be achieved through the application of two non-interacting inputs in the form of a voltage pulse and an illumination with high reproducibility of the output. The device hence acted as an OR logic gate and also stored the output state. In other words, the memristive device functioned as an OR gate implying an in-memory logic operation.

It is necessary to derive the truth table of a device based on a PPC material, namely $AgBiI_4$ for comparison. By defining the two inputs in the same manner as for devices based on the NPC-exhibiting material, the device-current has been presented in Fig. S10a.† The resistive state of the device as the output is in an LRS when (i) a +2.0 V (100 ms) has been applied and the device is probed under a dark condition (input: 00) and (ii) an illumination is shined (input: 01). The device was in an HRS if (iii) an electric pulse of −1.0 V (100 ms) under dark (input: 10) or (iv) both −1.0 V and illumination were imposed (input: 11). That is, the device could not be switched to the HRS by optical illumination alone. Due to the PPC in $AgBiI_4$, the output of the device with the voltage and optical illumination as the two inputs did not depict the truth table of a logic gate. In Fig. S10b,† we have presented the output state as a function of the two inputs in their four possible combinations. The results hence infer that resistive switching devices based only on an NPC-possessing material can effectively be used towards nonvolatile in-memory OR logic gate operations. Such devices could carry out the

(a) Inputs for the OR Gate

1st input (Electrical)		2nd input (Optical)	
0	1	0	1
+2.0 V (100ms)	-1.0 V (100ms)	Dark	Light (1sun, 1s)

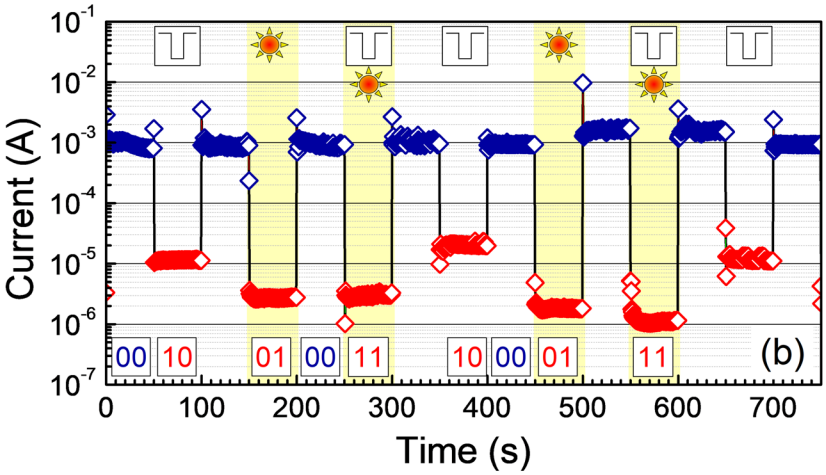

(c) Truth table of the OR Gate

Inputs		Outputs	
Electrical	Optical	Resistance (Ω)	State
0	0	211 (Low)	0
0	1	7×10^4 (High)	1
1	0	17×10^3 (High)	1
1	1	7×10^4 (High)	1

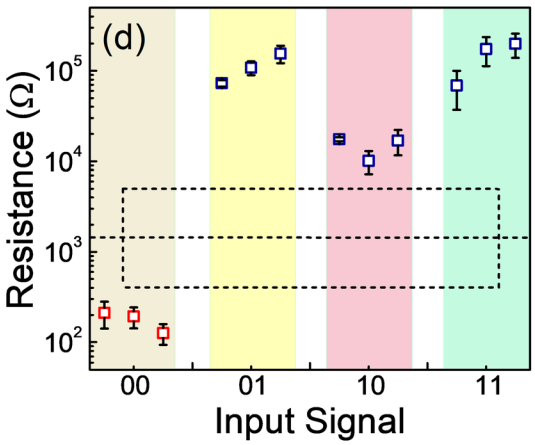

Fig. 5 (a) Specifications of the two input signals applied to the devices, (b) device current under a train of +0.2 V pulses after different combinations of independent electrical and optical inputs were imposed, (c) device resistance as the output under the application of the two inputs in the four combinations as a truth table, and (d) distribution of the device resistance under the four conditions for multiple tests (box-chart plot).

logic operation and thereafter store the output in the device itself.

It is imperative to touch upon the underlying mechanism of resistive switching, especially the optically reset characteristics, that is, the switching from an LRS to an HRS with the aid of illumination. It can be stated that most of the memristive devices based on halide perovskites show filamentary-type resistive switching where the switching process occurs due to the formation and rupture of single or multiple filaments as a result of electric-field-induced ion migrations.[20,43] Now, since such an ion-migration-induced phenomenon is independent of illumination,[44] the illumination may not cause rapture of metal filaments leading to the formation of an HRS or an optically reset process. Hence, the interface-type switching process, which is mostly dominated by trapping and detrapping of charge carriers at the interfacial defect states,[26,45] may have occurred in the devices. In such a process, the density of injected carriers, which increases with the bias, fills the trap-states leading to trap-filled limited conduction and lowering of the Schottky barrier at the interface and thereby an LRS. Under the reversal of the bias or exposure to illumination, these compensated carriers are detrapped or new trap-states are generated to restore the initial energy barrier and hence the HRS. Under illumination, photogenerated trap-states have led to a higher device resistance under illumination (input: 01) and also with both inputs (11) than the resistance under only the electrical input, that is, (10).

3. Conclusion

To summarize, this study demonstrates that a material exhibiting an NPC under illumination and voltage-induced resistive switching with an associated memory phenomenon can be envisaged for in-memory logic gate operations. In this work, we have considered silver-bismuth-iodide-based rudorffites; while all the rudorffites exhibited voltage-induced memristor characteristics, the silver-rich form, Ag_2BiI_5, evidenced an NPC due to photogeneration of trap states which took part in the recombination processes of photogenerated carriers and thereby an NPC. When the applied voltage and the illumination were applied to the sandwiched structures as two indepen-

dent inputs, the resistive state of the device has been the output of an OR logic gate, and the device retained the output state functioning both as a memory element and an OR gate, that is, an in-memory logic gate. The $AgBiI_4$ and bismuth-rich rudoffites, which yielded a PPC, did not function as a logic gate. An antagonism between the density of photogenerated carriers and the trap states has been found to determine the type of photoconductivity of the material that has been the key parameter towards achieving the in-memory OR logic gate operation.

4. Experimental section

4.1. Materials

Silver iodide (AgI, 99%), bismuth iodide (BiI_3, 99%), poly (methyl methacrylate) (PMMA), anhydrous *N*,*N*-dimethyl formamide (DMF, 99.8%), dimethylsulfoxide (DMSO), and 1,2-dichlorobenzene (DCB, anhydrous 99%) were purchased from Sigma-Aldrich Chemical Company; they were maintained in a chamber of a nitrogen-filled glovebox with both the moisture and oxygen level below 0.1 ppm. All the materials were used without any further purification.

4.2. Thin film formation and device fabrication

Thin films of the rudorffites in the silver-bismuth-iodide family were cast using a reported method. To do so, quartz and indium tin oxide (ITO) coated glass substrates were cleaned following the usual protocol through sonication in a liquid detergent, copious water, acetone, and isopropyl alcohol in sequence. The precursor solutions for the rudorffites were prepared in the glovebox by dissolving AgI and BiI_3 separately in a mixed solvent of DMF and DMSO (1 : 4 v/v). The solutions were stirred thoroughly overnight at 70 °C to form clear homogeneous stock solutions. Prior to the thin-film formation through a two-step spin coating method, the substrates were subjected to an ultraviolet ozone etching process to remove traces of organic residues. The precursor solutions, which were formed at different stoichiometric ratios, were spun in a spin-coater, which was fitted to the chamber of the glove box, on the substrates at 1000 rpm which was ramped after 10 s to 3500 rpm for the next 50 s. During the last ten seconds, 0.3 mL of dichlorobenzene was splashed as an antisolvent treatment process followed by drying in a vacuum for partial evaporation of the solvent; the films were finally annealed at 110 °C for 15 min and then heated to 160 °C for 15 min inside the glovebox. Through a variation in the stoichiometry of the precursors, we formed thin films of thermodynamically-stable Ag_2BiI_5, $AgBiI_4$, and $AgBi_2I_7$, rudorffites in the $A_mB_nX_{m+3n}$ series.

To prepare the devices, a thin PMMA layer was introduced on top of the perovskite layer. To do so, an 8 mg mL^{-1} PMMA solution in dichlorobenzene was spun on the perovskite film at 3500 rpm for 30 s. Finally, 100 nm-thick aluminum as the top electrode was thermally evaporated in a deposition chamber having a base pressure of 10^{-6} mbar. The process of thermal evaporation was carried out in the other chamber of the glovebox; the two chambers were connected through an antechamber.

4.3. Characterization of the thin films

After successful casting, the thin films of the compounds were characterized following the usual characterization techniques, such as UV-visible optical absorption spectroscopy and X-ray diffraction studies. A Shimadzu UV-2550 spectrophotometer and a Rigaku SmartLab X-ray diffractometer (Cu K_α radiation, λ = 1.54 Å) were used for the respective characterization studies. In addition, the surface morphology of the thin films was probed by recording atomic force microscopy (AFM) and scanning electron microscopy (SEM) images using a Nanosurf C300 atomic force microscope and a JEOL scanning electron microscope, respectively. The SEM images in the energy-dispersive X-ray mode were also used for elemental characterization of the thin films.

4.4. Device characterization

Current–voltage characteristics (*I*–*V*) of the devices were recorded in the other chamber of the glovebox, where the thermal evaporation unit was attached. Spring-loaded gold probes were used to make contact with the aluminum and ITO electrodes; a Keithley 2636 programmable electrometer operated through the LabView programming environment was used to record the *I*–*V* characteristics. A 300 W Solar Simulator (Newport-Stratfort model 76500) was used to record the characteristics under illumination conditions.

Conflicts of interest

There are no conflicts to declare.

Acknowledgements

A. J. P. acknowledges the JC Bose National Fellowship (JBR/2021/000001) and the Core Research Grant (CRG/2018/000183) of SERB and also the Asian Office of Aerospace Research and Development (AOARD) bearing a grant number FA2386-21-1-4031. S. P. acknowledges the CSIR NET Fellowship no. 09/080 (1107)/2019-EMR-I (roll number 528223).

References

1 C. H. Lui, A. J. Frenzel, D. V. Pilon, Y. H. Lee, X. Ling, G. M. Akselrod, J. Kong and N. Gedik, *Phys. Rev. Lett.*, 2014, **113**, 166801.
2 Y. X. Han, M. Q. Fu, Z. Q. Tang, X. Zheng, X. H. Ji, X. Y. Wang, W. J. Lin, T. Yang and Q. Chen, *ACS Appl. Mater. Interfaces*, 2017, **9**, 2867–2874.
3 N. K. Tailor, C. A. Aranda, M. Saliba and S. Satapathi, *ACS Mater. Lett.*, 2022, **4**, 2298–2320.

4 J. L. Sun, W. Zhang, J. L. Zhu and Y. Bao, *Opt. Express*, 2010, **18**, 4066–4073.
5 E. Baek, T. Rim, J. Schutt, C. K. Baek, K. Kim, L. Baraban and G. Cuniberti, *Nano Lett.*, 2017, **17**, 6727–6734.
6 P. C. Wei, S. Chattopadhyay, M. D. Yang, S. C. Tong, J. L. Shen, C. Y. Lu, H. C. Shih, L. C. Chen and K. H. Chen, *Phys. Rev. B: Condens. Matter Mater. Phys.*, 2010, **81**, 045306.
7 Y. M. Yang, X. Y. Peng, H. S. Kim, T. Kim, S. Jeon, H. K. Kang, W. Choi, J. D. Song, Y. J. Doh and D. Yu, *Nano Lett.*, 2015, **15**, 5875–5882.
8 W. B. Niu, H. Chen, R. Chen, J. F. Huang, H. D. Sun and A. I. Y. Tok, *Chem. Commun.*, 2015, **51**, 9030–9033.
9 J. Y. Wu, Y. T. Chun, S. P. Li, T. Zhang, J. Z. Wang, P. K. Shrestha and D. P. Chu, *Adv. Mater.*, 2018, **30**, 1705880.
10 C. Biswas, F. Güneş, D. D. Loc, S. C. Lim, M. S. Jeong, D. Pribat and Y. H. Lee, *Nano Lett.*, 2011, **11**, 4682–4687.
11 J. N. Heyman, J. D. Stein, Z. S. Kaminski, A. R. Banman, A. M. Massari and J. T. Robinson, *J. Appl. Phys.*, 2015, **117**, 015101.
12 A. Grillo, E. Faella, A. Pelella, F. Giubileo, L. Ansari, F. Gity, P. K. Hurley, N. McEvoy and A. Di Bartolomeo, *Adv. Funct. Mater.*, 2021, **31**, 2105722.
13 E. Faella, K. Intonti, L. Viscardi, F. Giubileo, A. Kumar, H. T. Lam, K. Anastasiou, M. F. Craciun, S. Russo and A. Di Bartolomeo, *Nanomaterials*, 2022, **12**, 1886.
14 M. A. Hague, J. L. Li, A. L. Abdelhady, M. I. Saidaminov, D. Baran, O. M. Bakr, S. H. Wei and T. Wu, *Adv. Opt. Mater.*, 2019, **7**, 1900865.
15 H. N. Jin, Y. B. Chen, L. W. Zhang, R. Wan, Z. G. Zou, H. X. Li and Y. H. Gao, *Nanotechnology*, 2021, **32**, 085202.
16 Q. Q. He, G. Y. Chen, Y. K. Wang, X. Y. Liu, D. T. Xu, X. X. Xu, Y. Liu, J. C. Bao and X. Wang, *Small*, 2021, **17**, 2101403.
17 N. K. Tailor, P. Maity, M. I. Saidaminov, N. Pradhan and S. Satapathi, *J. Phys. Chem. Lett.*, 2021, **12**, 2286–2292.
18 N. K. Tailor, P. Maity and S. Satapathi, *ACS Photonics*, 2021, **8**, 2473–2480.
19 Y. Wang, E. Liu, A. Gao, T. Cao, M. Long, C. Pan, L. Zhang, J. Zeng, C. Wang, W. Hu, S.-J. Liang and F. Miao, *ACS Nano*, 2018, **12**, 9513–9520.
20 X. Y. Xiao, J. Hu, S. Tang, K. Yan, B. Gao, H. L. Chen and D. C. Zou, *Adv. Mater. Technol.*, 2020, **5**, 1900914.
21 Y. Fang, S. Zhai, L. Chu and J. Zhong, *ACS Appl. Mater. Interfaces*, 2021, **13**, 17141–17157.
22 L. Gao, Q. Ren, J. Sun, S.-T. Han and Y. Zhou, *J. Mater. Chem. C*, 2021, **9**, 16859–16884.
23 Z. G. Xiao and J. S. Huang, *Adv. Electron. Mater.*, 2016, **2**, 1600100.
24 B. X. Li, W. Hui, X. Q. Ran, Y. D. Xia, F. Xia, L. F. Chao, Y. H. Chen and W. Huang, *J. Mater. Chem. C*, 2019, **7**, 7476–7493.
25 S. Paramanik and A. J. Pal, *Adv. Electron. Mater.*, 2022, **8**, 2200211.
26 A. P. Chen, W. R. Zhang, L. R. Dedon, D. Chen, F. Khatkhatay, J. L. MacManus-Driscoll, H. Y. Wang, D. Yarotski, J. Chen, X. S. Gao, L. W. Martin, A. Roelofs and Q. X. Jia, *Adv. Funct. Mater.*, 2020, **30**, 2000664.
27 M. Di Ventra and Y. V. Pershin, *Nat. Phys.*, 2013, **9**, 200–202.
28 Q. F. Ou, B. S. Xiong, L. Yu, J. Wen, L. Wang and Y. Tong, *Materials*, 2020, **13**, 3532.
29 L. Yin, R. Q. Cheng, Y. Wen, C. S. Liu and J. He, *Adv. Mater.*, 2021, **33**, 2007081.
30 J. X. Pei, X. H. Wu, W. J. Liu, D. W. Zhang and S. J. Ding, *ACS Nano*, 2022, **16**, 2442–2451.
31 I. Turkevych, S. Kazaoui, E. Ito, T. Urano, K. Yamada, H. Tomiyasu, H. Yamagishi, M. Kondo and S. Aramaki, *ChemSusChem*, 2017, **10**, 3754–3759.
32 A. Chakraborty, N. Pai, J. Zhao, B. R. Tuttle, A. N. Simonov and V. Pecunia, *Adv. Funct. Mater.*, 2022, **32**, 2203300.
33 A. Bera, S. Paramanik, A. Maiti and A. J. Pal, *Phys. Rev. Mater.*, 2021, **5**, 095404.
34 F. Urban, F. Gity, P. K. Hurley, N. McEvoy and A. D. Bartolomeo, *Appl. Phys. Lett.*, 2020, **117**, 193102.
35 J.-L. Li, J. Yang, T. Wu and S.-H. Wei, *J. Mater. Chem. C*, 2019, **7**, 4230–4234.
36 W. Nie, J. C. Blancon, A. J. Neukirch, K. Appavoo, H. Tsai, M. Chhowalla, M. A. Alam, M. Y. Sfeir, C. Katan, J. Even, S. Tretiak, J. J. Crochet, G. Gupta and A. D. Mohite, *Nat. Commun.*, 2016, **7**, 11574.
37 M. Khazaee, K. Sardashti, C. C. Chung, J. P. Sun, H. H. Zhou, E. Bergmann, W. A. Dunlap-Shohl, Q. W. Han, I. G. Hill, J. Jones, D. C. Lupascu and D. B. Mitzi, *J. Mater. Chem. A*, 2019, **7**, 2095–2105.
38 G. Gordillo, C. A. Otalora and A. A. Ramirez, *Phys. Chem. Chem. Phys.*, 2016, **18**, 32862–32867.
39 A. Poglitsch and D. Weber, *J. Chem. Phys.*, 1987, **87**, 6373–6378.
40 D. Shi, V. Adinolfi, R. Comin, M. J. Yuan, E. Alarousu, A. Buin, Y. Chen, S. Hoogland, A. Rothenberger, K. Katsiev, Y. Losovyj, X. Zhang, P. A. Dowben, O. F. Mohammed, E. H. Sargent and O. M. Bakr, *Science*, 2015, **347**, 519–522.
41 X. Zou, H. G. Ong, L. You, W. Chen, H. Ding, H. Funakubo, L. Chen and J. Wang, *AIP Adv.*, 2012, **2**, 032166.
42 Z. H. Liu, P. P. Cheng, Y. F. Li, R. Y. Kang, Z. Q. Zhang, Z. Y. Zuo and J. Zhao, *ACS Appl. Mater. Interfaces*, 2021, **13**, 58885–58897.
43 T. Li, H. L. Yu, S. H. Y. Chen, Y. Zhou and S. T. Han, *J. Mater. Chem. C*, 2020, **8**, 16295–16317.
44 W. Tress, N. Marinova, T. Moehl, S. M. Zakeeruddin, M. K. Nazeeruddin and M. Gratzel, *Energy Environ. Sci.*, 2015, **8**, 995–1004.
45 A. Rana, H. D. Lu, K. Bogle, Q. Zhang, R. Vasudevan, V. Thakare, A. Gruverman, S. Ogale and N. Valanoor, *Adv. Funct. Mater.*, 2014, **24**, 3962–3969.